Supporting Information

Influence of the central diamagnetic cyanidometal on the distant magnetic interaction in cyanide-bridged Fe(III)-M(II)-Fe(III) complexes?

Yong Wang,[a] Chensheng Lin,[a] Xiao Ma,[a] Zhenzhen Xue,[a] Xiaoquan Zhu,[a] Wenhai Cao,[a] Shengmin Hu,[a] Tianlu Sheng,*[a] and Xintao Wu[a]

[a] State Key Laboratory of Structure Chemistry, Fujian Institute of Research on the Structure of Matter, Chinese Academy of Sciences, Fuzhou, 350002, Fujian, P.R. China

TDDFT Calculations

For the singly oxidized species **5** and **6**, it is difficult to attribute the absorption bands in the NIR region, because three assignments are possible: 1) the central Os^{II}→ terminal Fe^{III} MMCT; 2) the distant terminal Fe^{II}→ terminal Fe^{III} MMCT; 3) the mixture of the central Os^{II}→ terminal Fe^{III} and the terminal Fe^{II}→ terminal Fe^{III} MMCTs. In order to accurately assign the absorption bands in the NIR regions of **5** and **6**, the TDDFT calculations have been done. The redistributions of electron densities are shown in Figures S3 and S4 for **5** and **6**, respectively. The frontier orbitals of complexes **5** and **6** in the CH_3CN solution are shown in Figures S5-S8. The calculated vertical excitation energies and contribution of complexes **5** and **6** are listed in Table S1. The calculated maximum absorption wavelengths in the NIR region are 819.7 nm for **5** and 823.2 nm for **6**, respectively. These are in accordance with the experimental data (910 nm for **5** and 912 nm for **6**). From the redistribution of electron densities (Figures S3 and S4), it can be found that the flow of electrons largely comes from the mixture of the central Os^{II}→ terminal Fe^{III} and the distant terminal Fe^{II}→ terminal Fe^{III} MMCTs. Furthermore, the frontier molecular orbital analysis indicates that the broad band at 910 nm for **5** and 912 nm for **6** are mainly assigned to the molecular orbital β electron HOMO-1→LUMO transition.

Computational Methods.

All calculations have been performed with the Gaussian 09 program package. The geometry of complexes **5** and **6** were optimized at the B3LYP level with LANL2DZ basis set for atoms C, H, N, Os

and Fe and 6-31+G* basis set for atom P. TDDFT calculation was done based on these optimized structure. The solvent effect (acetonitrile) was taken into account by using the PCM approximation[1] in these calculations.

[1] R. Improta, V. Barone, G. Scalmani, M. J. Frisch, *J. Chem. Phys.* **2006**, *125*, 054103: 054101-054109.

Table S1. Crystallographic Data and Details of Structure Determination for **1-3**.

	1·$2Et_2O·CH_2Cl_2$	**2**·$4CH_2Cl_2$	**3**·$2CH_2Cl_2·C_4H_{10}O$
Chemical formula	$C_{93}H_{96}Cl_2F_{12}Fe_2N_6O_2OsP_6$	$C_{92}H_{82}Cl_8F_{12}Fe_2N_6OsP_6$	$C_{90}H_{88}Cl_4F_{12}Fe_3N_6P_6$
Formula weight	2116.38	2270.96	1992.83
Colour and Habit	Red needle	Red needle	Gray prism
Crystal Size / mm	0.45×0.04×0.03	0.56×0.05×0.04	0.79×0.17×0.05
T / K	123	123	123
Crystal system	Monoclinic	Orthorhombic	Monoclinic
Space group	$P2_1/n$	$Pbca$	$P2_1/c$
a / Å	11.259(7)	28.108(11)	11.294(5)
b /Å	34.410(18)	20.092(8)	33.956(14)
c / Å	23.606(14)	33.297(14)	25.136(10)
α / °	90.00	90.00	90.00
β / °	95.685(12)	90.00	110.097(17)
γ / °	90.00	90.00	90.00
V / Å^3	9100(9)	18804(13)	9053(7)
Z	4	8	4
ρ_{calcd}(g/cm^3)	1.545	1.604	1.462
λ (Mo K_α, Å)	0.71073	0.71073	0.71073
μ(Mo K_α, mm^{-1})	1.948	2.055	0.773
Completeness	98.1%	98.1%	98.3%
F(000)	4288	9104	4088
h, k, l, range	-13≤h≤13, -40≤k≤40, -28≤l≤28	-33≤h≤33, -23≤k≤23, -39≤l≤39	-12≤h≤14, -42≤k≤44, -32≤l≤32
θ range / deg	2.70-25.00	2.12-25.00	2.01-27.50
Reflections measured	15727	16241	20455
R_{int}	0.0946	0.1451	0.1141
Params/restraints/ Data(obs.)	1171/708/11833	1180/117/11594	1182/191/11924
GOF	1.047	1.064	1.012

R_1, $_\omega R_2$ (I >2 $\sigma(I)$)	0.0989, 0.1993	0.1132, 0.2050	0.1069, 0.2104
R_1, $_\omega R_2$ (all data)	0.1254, 0.2151	0.1418, 0.2239	0.1488, 0.2354

Table S2. Selected Bond Distances (Å) and Bond Angles (°) for **1-3.**

	1	**2**		**3**
Os-C1	1.953(13)	1.997(13)	Fe3-C1	1.932(7)
Os-C2	1.976(14)	2.003(13)	Fe3-C2	1.921(7)
Os-N3	2.105(10)	2.111(9)	Fe3-N3	1.984(4)
Os-N4	2.064(10)	2.070(10)	Fe3-N4	1.998(6)
Os-N5	2.052(10)	2.090(10)	Fe3-N5	1.983(5)
Os-N6	2.074(10)	2.106(9)	Fe3-N6	1.984(5)
C1≡N1	1.233(15)	1.171(14)	C1≡N1	1.157(8)
C2≡N2	1.199(15)	1.181(14)	C2≡N2	1.155(8)
Fe1-N1	1.905(10)	1.898(9)	Fe1-N1	1.930(6)
Fe2-N2	1.907(10)	1.902(9)	Fe2-N2	1.921(5)
Fe1-P1	2.197(4)	2.200(4)	Fe1-P1	2.205(2)
Fe1-P2	2.189(5)	2.195(3)	Fe1-P2	2.191(2)
Fe2-P3	2.202(4)	2.195(4)	Fe2-P3	2.212(2)
Fe2-P4	2.192(4)	2.189(3)	Fe2-P4	2.193(2)
C1-Os-C2	94.2(5)	92.1(4)	C1-Fe3-C2	91.9(3)
N1≡C1-Os	179.3(11)	177.2(10)	N1≡C1-Fe3	174.4(6)
N2≡C2-Os	176.7(10)	177.7(10)	N2≡C2-Fe3	172.4(6)
C1≡N1-Fe1	171.0(9)	178.6(10)	C1≡N1-Fe1	174.7(5)
C2≡N2-Fe2	178.2(10)	173.7(9)	C2≡N2-Fe2	176.2(5)
Os···Fe1	5.091	5.066	Fe3···Fe1	5.019
Os···Fe2	5.082	5.084	Fe3··Fe2	5.000
Fe1···Fe2	7.652	7.592	Fe1···.Fe2	7.602
Fe1···Fe2(-NC-Os-CN)	10.173	10.150	Fe1···Fe2(-NC-Fe-CN)	10.019

Table S3. Calculated Vertical Excitation Energies in nm for Complexes **5** and **6**.

5, α electron (HOMO: 363α; LUMO: 364α), β electron (HOMO: 362β; LUMO: 363β)		**6**, α electron (HOMO: 375α; LUMO: 364α), β electron (HOMO: 362β; LUMO: 363β)	
λ(nm)	Contribution (coefficient)	λ(nm)	Contribution (coefficient)
819.7	337α→364α (-0.11995), 337α→365α (-0.33109), 359α→365α (-0.14635); 360α→ 365α (-0.18472), 362α→365α (-0.10596), 363α→365α (-0.14818), 353β→ 367β (-0.17830), 356β→367β (0.10701),	823.2	347α→ 376α (0.10944), 347α→377α (0.28429), 371α→377α (0.12562), 372α→377α (-0.16878), 374α→377α (0.10700), 375α→377α (-0.13084), 366β→381β (0.13656), 368β→381β (0.11943),

	357β→363β (-0.21621), 359β→ 363β (-0.37658), 360β→363β (-0.11318), 360β→367β (-0.11735), 361β→363β (0.62523).		369β →375β (0.21569), 371β→375β (0.36866), 372β →375β (0.12996), 372β→381β (-0.10814), 373β→375β (0.65943).

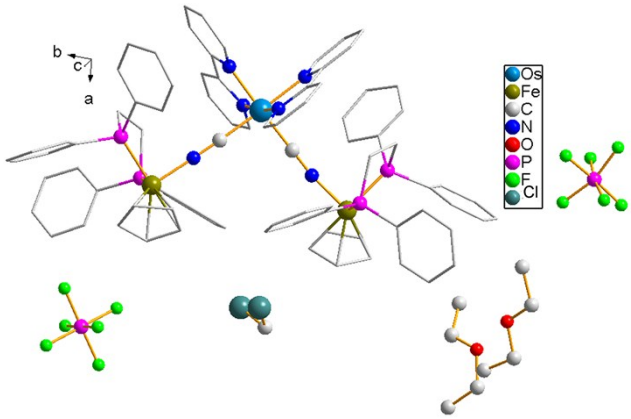

Figure S1. Molecular structure of **1**, hydrogen atoms have been removed for clarity.

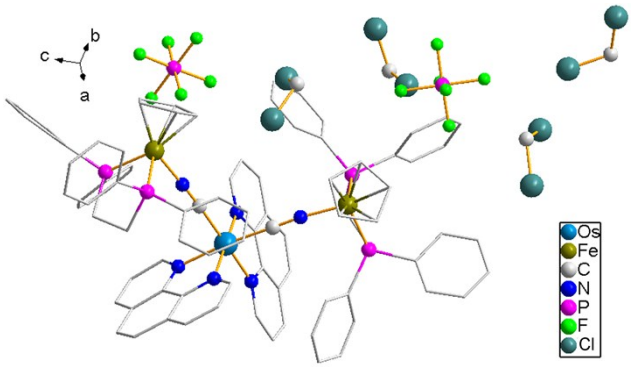

Figure S2. Molecular structure of **2**, hydrogen atoms have been removed for clarity.

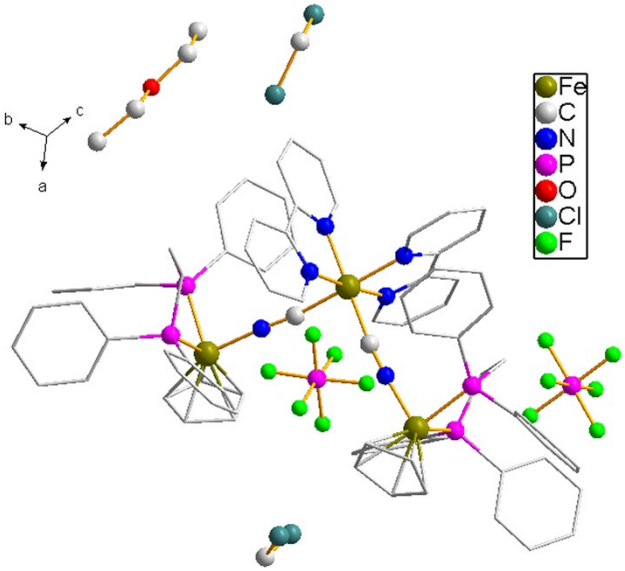

Figure S3. Molecular structure of **3**, hydrogen atoms have been removed for clarity.

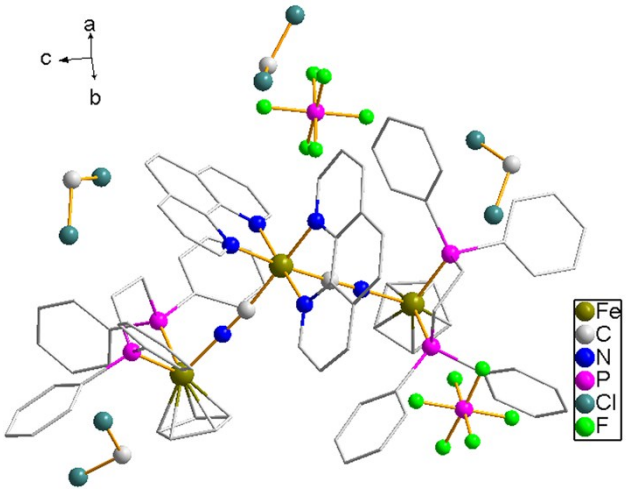

Figure S4. Molecular structure of **4**, hydrogen atoms have been removed for clarity.

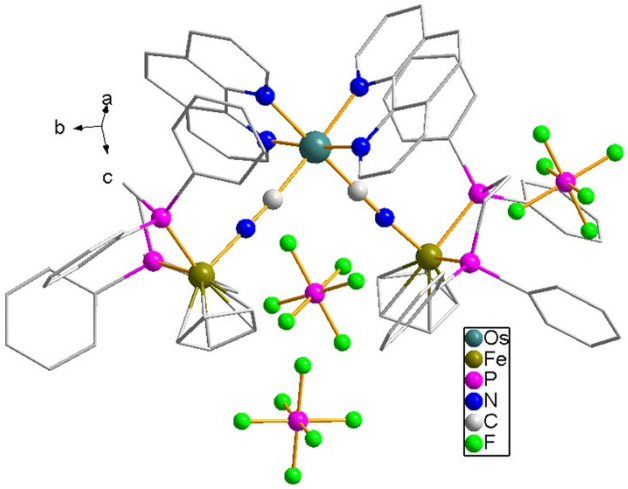

Figure S5. Molecular structure of **6**, hydrogen atoms have been removed for clarity.

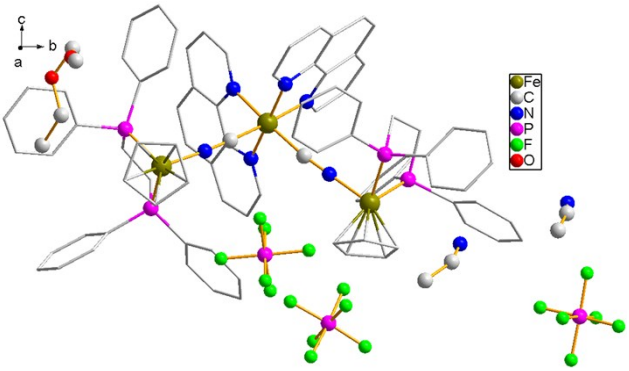

Figure S6. Molecular structure of **7**, hydrogen atoms have been removed for clarity.

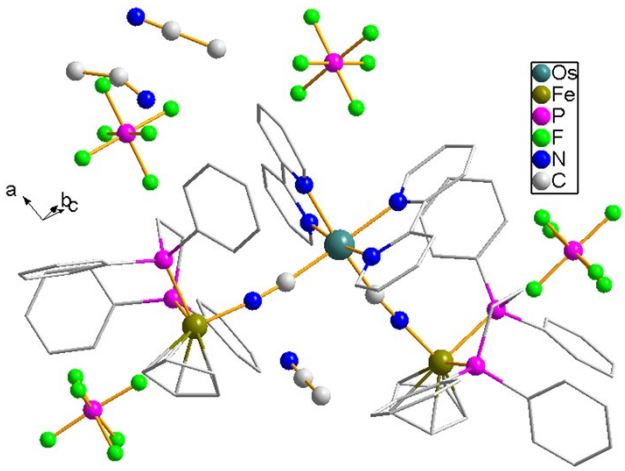

Figure S7. Molecular structure of **8**, hydrogen atoms have been removed for clarity.

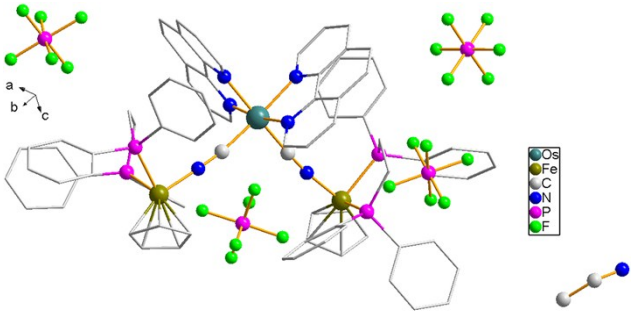

Figure S8. Molecular structure of **9**, hydrogen atoms have been removed for clarity.

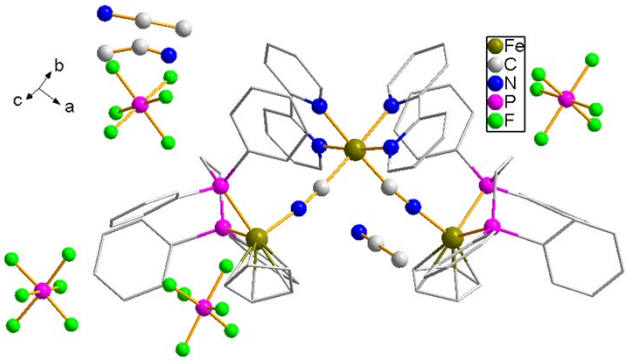

Figure S9. Molecular structure of **10**, hydrogen atoms have been removed for clarity.

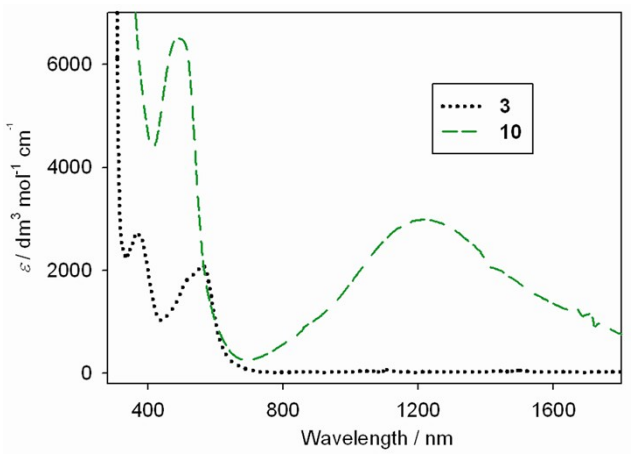

Figure S10. Electronic absorption spectra of complexes **3** and **10** in CH_3CN at room temperature.

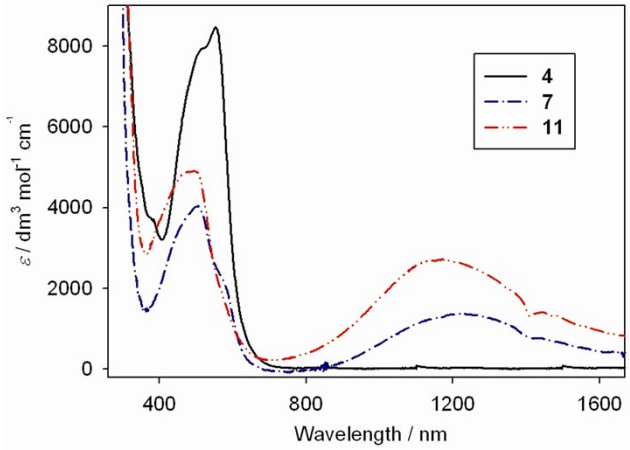

Figure S11. Electronic absorption spectra of complexes **4**, **7** and **11** in CH_3CN at room temperature.

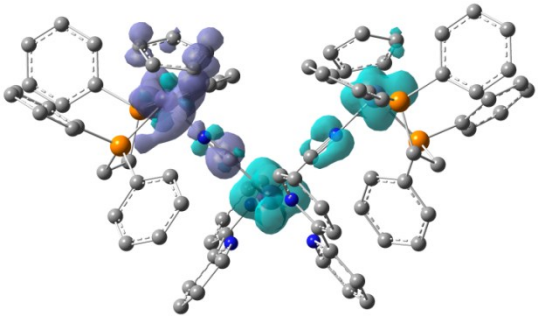

Figure S12. Redistribution of electron densities of **5** in the calculated 819.7 nm transition band. represents gain of electron density and represents losses of electron density after transition. The electron density value corresponds to the sosurface of 0.001.

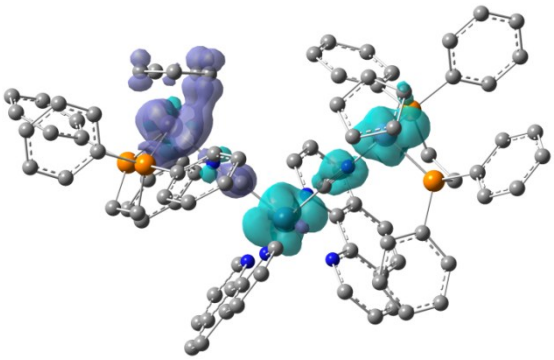

Figure S13. Redistribution of electron densities of **6** in the calculated 823.2 nm transition band. represents gain of electron density and represents losses of electron density after transition. The electron density value corresponds to the sosurface of 0.001.

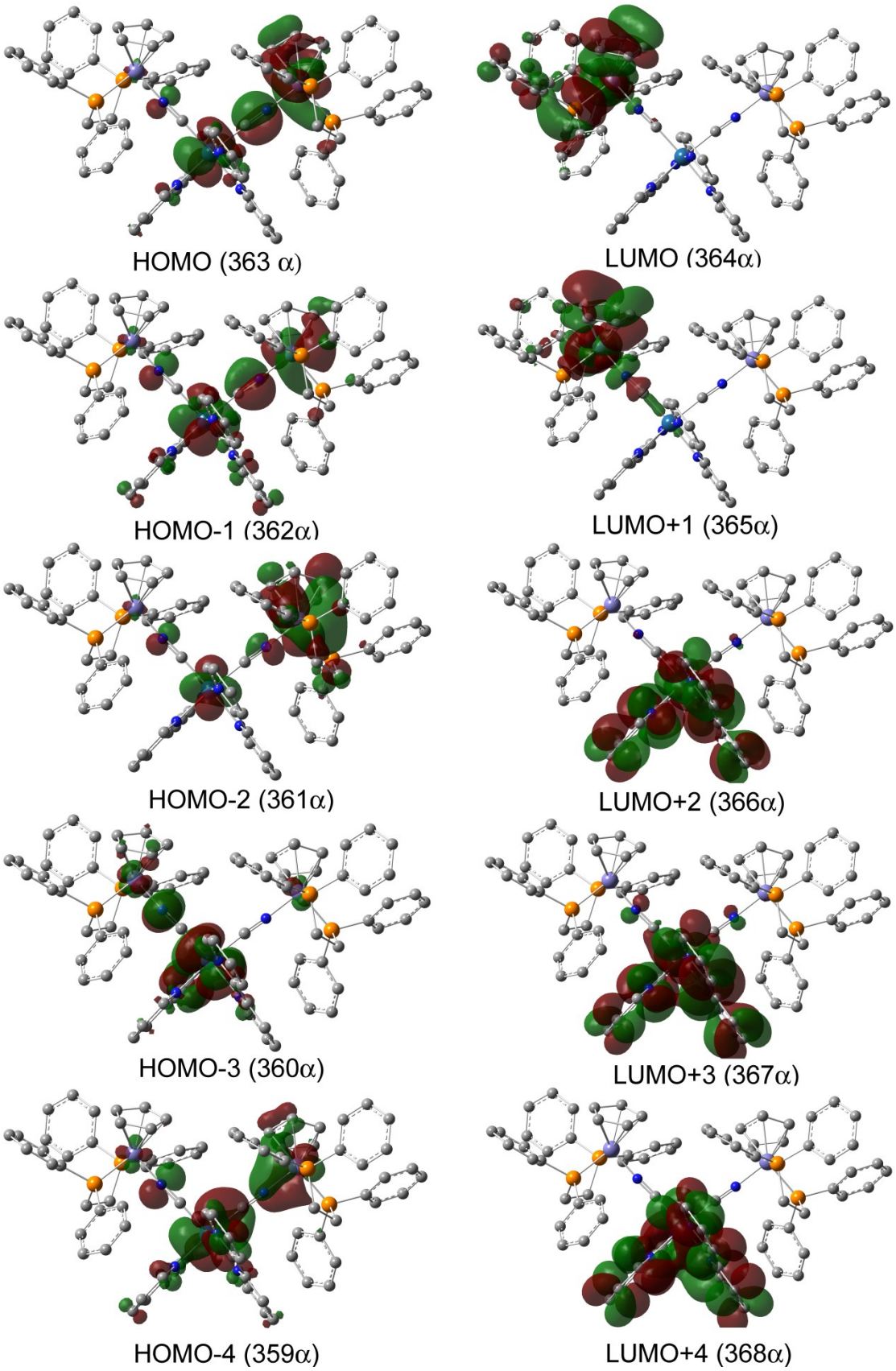

Figure S14. Schematic drawings of the selective frontier molecular orbitals for the α electron of **5**.

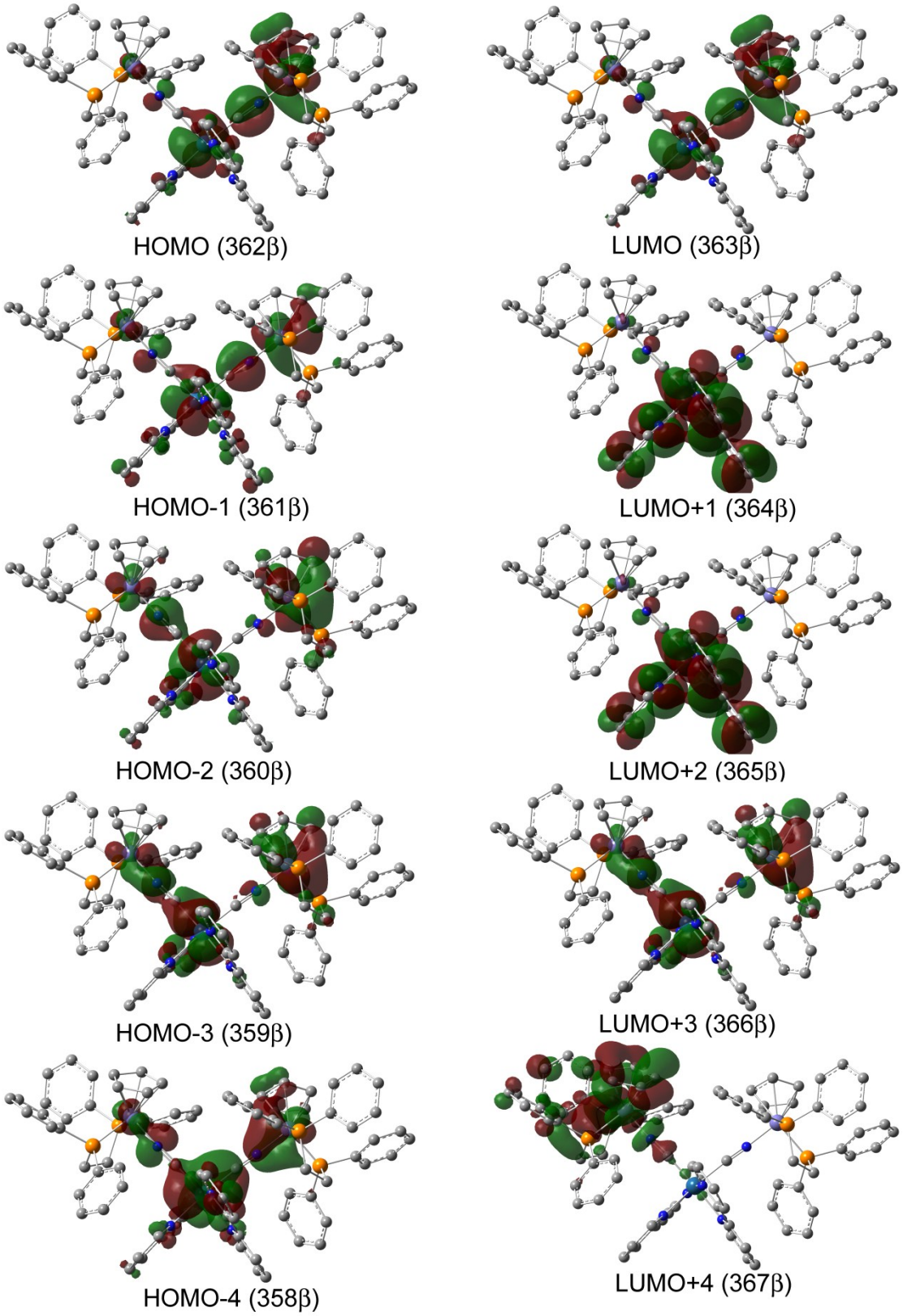

Figure S15. Schematic drawings of the selective frontier molecular orbitals for the β electron of **5**.

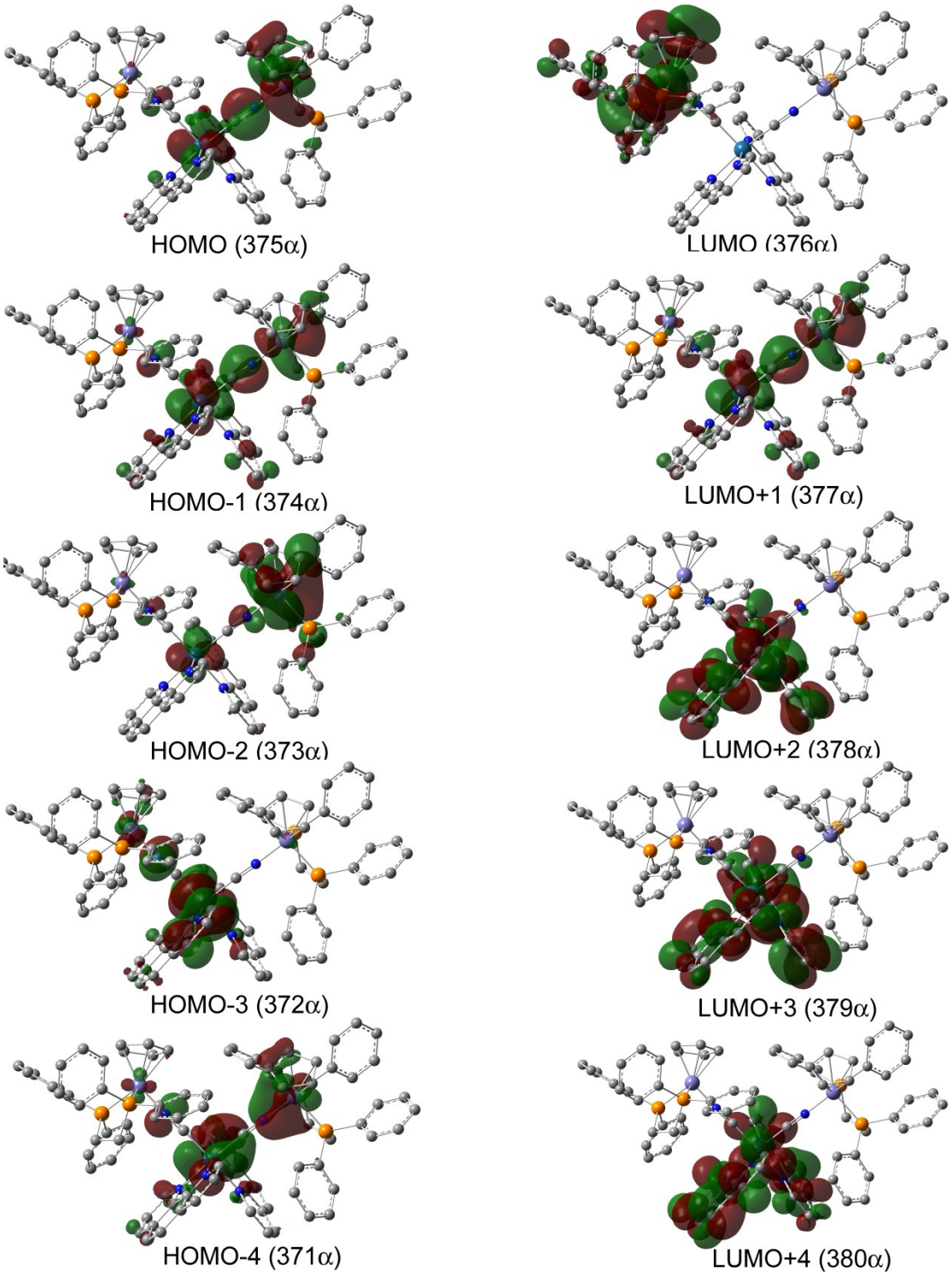

Figure S16. Schematic drawings of the selective frontier molecular orbitals for the α electron of **6**.

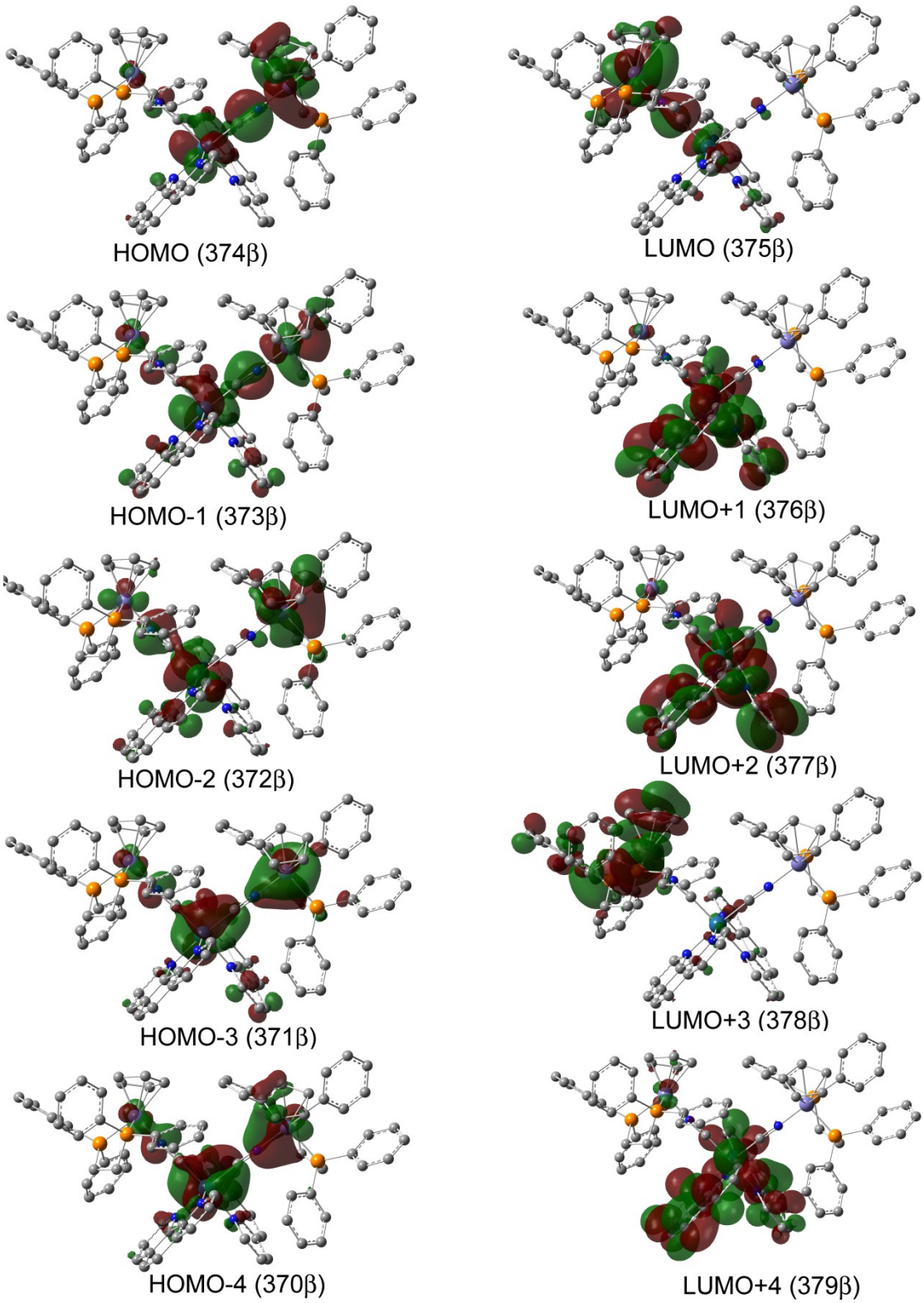

Figure S17. Schematic drawings of the selective frontier molecular orbitals for the β electron of **6**.

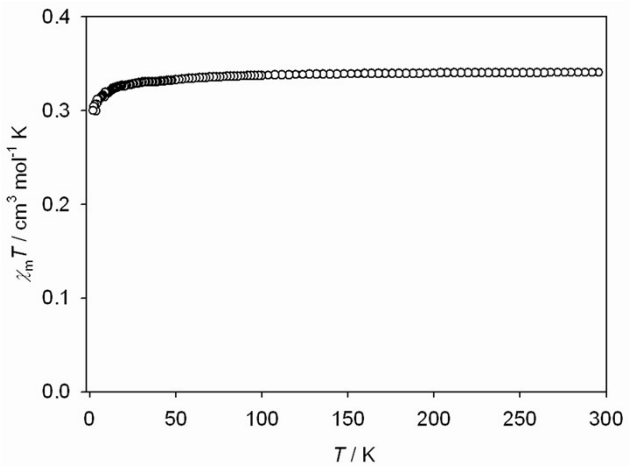

Figure S18. Magnetic behavior of complex **5** as measured in an applied field of 1000 Oe using a SQUID magnetometer. Temperature dependence of $\chi_M T$ of complex **5** in polycrystalline sample.

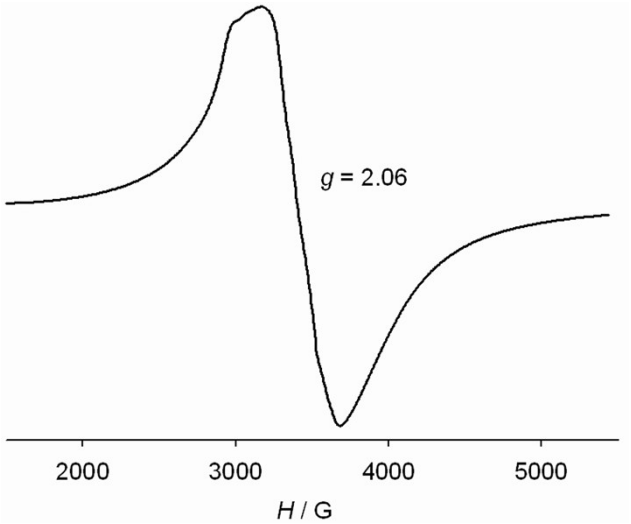

Figure S19. EPR spectra of complex **5** in polycrystalline sample at room temperature.

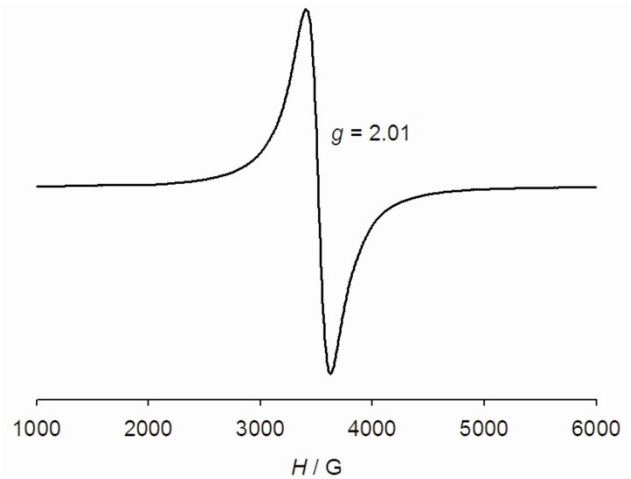

Figure S20. EPR spectra of complex **8** in solid sample at room temperature.

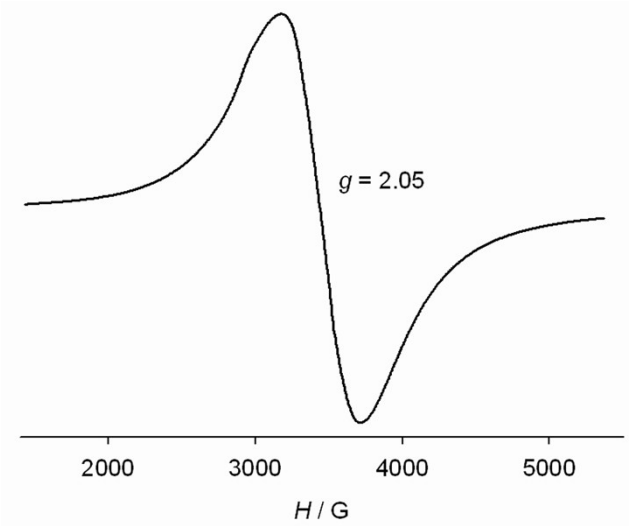

Figure S21. EPR spectra of complex **6** in polycrystalline sample at room temperature.

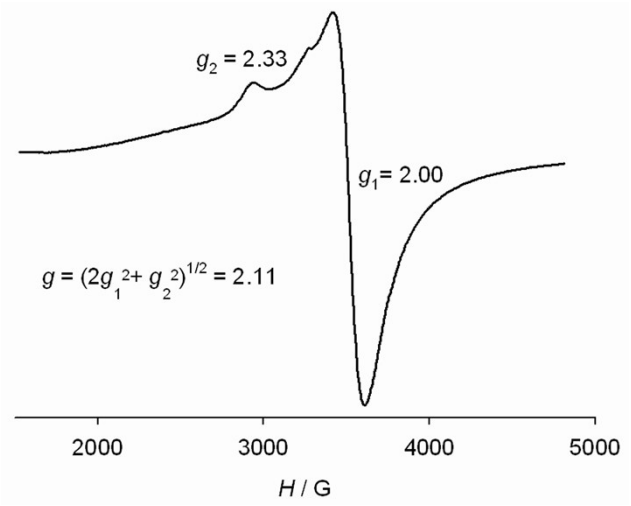

Figure S22. EPR spectra of complex **9** in polycrystalline sample at room temperature.

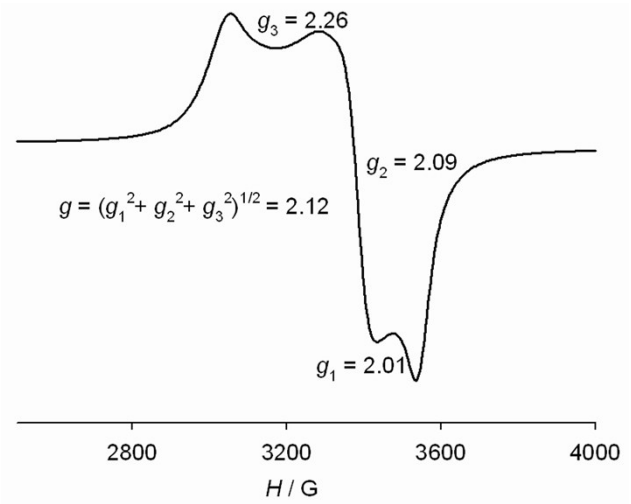

Figure S23. EPR spectra of complex **10** in polycrystalline sample at room temperature.

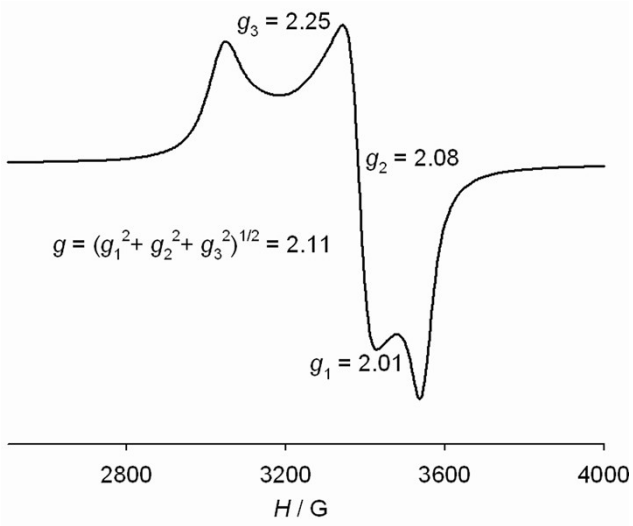

Figure S24. EPR spectra of complex **11** in polycrystalline sample at room temperature.

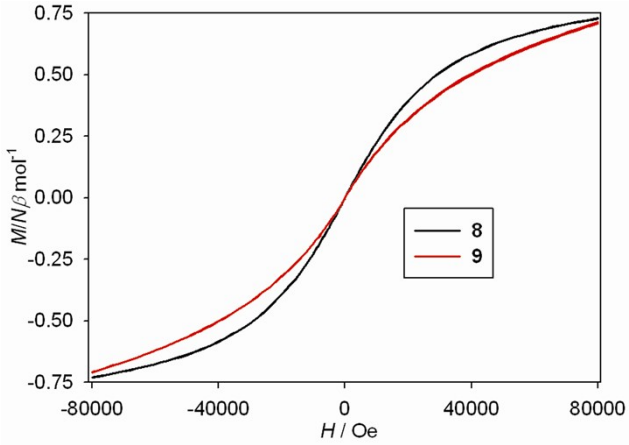

Figure S25. Plots of M-H for samples **8** and **9** at 2 K.